

Radar and electrical characteristics of convection observed during MCTEX

David A. Ahijevych, Steven A. Rutledge and Lawrence D. Carey
Department of Atmospheric Science, Colorado State University, Fort Collins,
Colorado

(Manuscript received September 1999; revised March 2000)

The Maritime Continent Thunderstorm Experiment (MCTEX) was conducted over the Tiwi Islands 50-100 km north of Darwin, Australia, during November-December 1995. Two MCTEX cases are presented in this study. First, the convective evolution is summarised, including the processes by which shallow precipitating cumulus clouds evolved into electrically active, deep convection. Using multiparameter radar (C-band; 5.3 cm) estimates, the history of precipitation-sized ice and liquid water is compared to lightning-flash rates. In this context, the non-inductive graupel-ice particle charging theory is evaluated.

For both case study days, the first deep convection was anchored to the leeward coast sea-breeze front. First, shallow precipitating cells originating from the island interior created evaporatively cooled pools that focused surface convergence along their perimeter. Rapid convective development ensued as these cool pools approached the sea-breeze front, triggering higher order cloud mergers along the sea-breeze front. This vigorous deep convection produced an extensive cold pool with convection persisting along its western edge where the environmental wind shear enabled more vertically oriented updraughts.

The temporal evolution of mixed-phase graupel mass was compared to lightning-flash rates. Lightning was detected only after convective cells produced significant quantities of millimeter-sized ice particles. Lightning was not detected in predominately warm-rain cells. Furthermore, fluctuations in graupel mass were correlated with fluctuations in lightning-flash rates. Cloud-to-ground lightning was found to be closely tied to the mixed-phase graupel mass, consistent with the non-inductive graupel-ice particle charging theory. Polarimetric radar estimates also suggested that graupel formed as raindrops were lofted above the freezing level by convective updraughts.

Introduction

Our understanding of tropical convection has grown substantially in recent years due to several comprehensive field campaigns. The Global Atmosphere

Research Program (GARP), Atlantic Tropical Experiment GATE, the Tropical Ocean-Global Atmosphere (TOGA) Coupled Ocean-Atmosphere Response Experiment (COARE) (Webster and Lucas 1992), the Central Pacific Equatorial Experiment (CEPEX 1993), and the Equatorial Mesoscale Experiment (EMEX; Webster and House 1991; Gamache et al. 1987) all provided new insights in understanding tropical oceanic convection. The

Corresponding author address: Dr. Steven A. Rutledge, Department of Atmospheric Science, Colorado State University, Fort Collins, CO, USA, 80523-1371.
e-mail: rutledge@radarmet.atmos.colostate.edu

Venezuelan International Meteorological and Hydrological Experiment (VIMHEX; Miller and Betts 1977), the Convection Profonde Tropicale (COPT81) experiment (Sommeria and Testud 1984), the Australian Monsoon Experiment (AMEX; Holland et al. 1986), the Down Under Doppler and Electricity Experiment (DUNDEE; Rutledge et al. 1992), and the Tropical Rainfall Measurement Mission – Large Scale Biosphere-Atmosphere Experiment (TRMM-LBA)/Brazil Project have advanced our understanding of tropical continental convection. Observational gaps in the remaining class of tropical convection, island convection, were partly filled by the Island Thunderstorm Experiment (ITEX; Keenan et al. 1989), winter monsoon experiment (Winter MONEX; Houze et al. 1981), and the program on which this study is based, the Maritime Continent Thunderstorm Experiment (MCTEX) (Keenan et al. 1994a, 1996a, 2000).

Some of the deepest convection in the world occurs over the Indonesian Archipelago, where myriad islands act as ‘hot plates’ for the tropical atmosphere. Taken as a whole, this conglomeration of thunderstorm activity over the ‘maritime continent’ (Ramage 1968) approaches the spatial scale of the Rossby radius of deformation and provides primary forcing for the Hadley and Walker circulations (Krishnamurti et al. 1973; Janowiak et al. 1985; Rasmusson and Arkin 1985). The amount of convective activity in this region is closely related to the El Niño-Southern Oscillation phenomenon and has been shown to influence the behaviour of the subtropical jet on a daily basis (Lau et al. 1983). Additional studies have provided evidence that these vigorous thunderstorms are central to maintaining the global electrical circuit (Williams et al. 1990; Rutledge et al. 1992), in addition to being a key component of the global circulation.

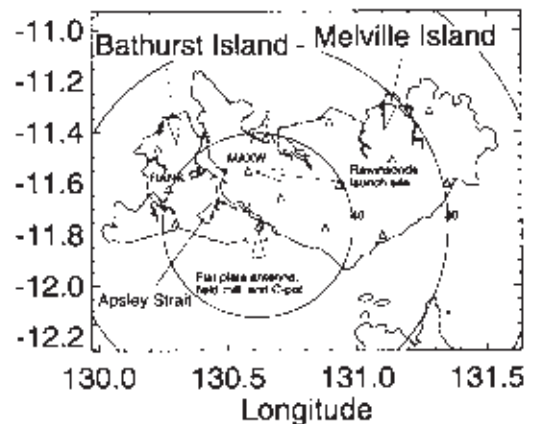
Strongly influenced by diurnal and coastal effects, thunderstorms occur regularly over Indonesia and tropical northern Australia. Over the Tiwi Islands, north of Darwin, in Australia's Northern Territory, deep convection is often spawned by a combination of land heating and sea-breeze convergence (Skinner and Tapper 1994; Carbone et al. 2000). In the early afternoon, shallow precipitating cells develop over the island interior. The sea-breeze front of the leeward coast plays a dominant role in subsequent cell mergers and rapid upscale development (Simpson et al. 1993; Carbone et al. 2000). The end result is often a mesoscale system for which new convective development is favored at the intersection of its gust front and pre-existing boundaries (Carbone et al. 2000). The mesoscale system, in the form of a small squall line, propagates to the west with the surface to 700

hPa steering flow (Keenan et al. 1990; Keenan and Carbone 1992; Carbone et al. 2000). MCTEX was designed to study the lifecycle of these island storms in an effort to improve understanding of similar phenomena found over the hundreds of other islands dotted across the ‘maritime continent’. As stated in the MCTEX science plan (Keenan et al. 1994a), the basic science objective was ‘to improve knowledge of the dynamics and interaction of the physical processes involved in the organization and life cycle of tropical island convection over the Maritime Continent and the role of this convection in the atmospheric energy and moisture balance’.

During MCTEX, a C-band dual-polarimetric radar (C-pol) was positioned at Nguiu, on Bathurst Island (Fig. 1). The radar was used in conjunction with a lightning detection network to document the micro-physical and electrical life cycle of the island thunderstorms. This included the shallow precipitating cumulus stage, the rapid development near the sea-breeze front, subsequent merger along the sea-breeze front and finally the dissipation stage.

Herein, special emphasis is placed on testing the non-inductive graupel-ice particle charging theory (hereafter referred to as NIC). This thunderstorm electrification theory is based on laboratory studies which have suggested that graupel particles become significantly charged when they undergo collisions with smaller ice crystals in the presence of super-cooled water (e.g. Reynolds et al. 1957; Takahashi

Fig. 1 Map of Tiwi Islands with range rings (km) centered on the C-pol radar. Automated weather stations (AWS) are denoted by triangles. Latitude and longitude are in degrees throughout this study.



1978; Jayaratne et al. 1983; Saunders et al. 1991; Avila and Caranti 1994). To test this theory, lightning-flash rates are compared to the evolution of total graupel mass in the mixed-phase region (between the 0°C and -40°C levels).

According to NIC theory, in order for lightning to be produced, a significant concentration of graupel must reside above the freezing level in the presence of small ice crystals and supercooled cloud droplets. Emerging from this mixture of interacting particles are two oppositely charged hydrometeor populations, graupel and ice crystals. The two populations separate due to dissimilar fall speeds, thereby generating an electric dipole. Although the C-pol radar is relatively insensitive to supercooled cloud droplets and ice crystals, the radar can infer the amount of graupel present. Since NIC theory requires graupel in the mixed-phase region before lightning can occur, radar-estimated mixing ratios of graupel correlated to lightning-flash rates can provide an indirect test of the NIC theory. This test will be one of the central aims of this present study. This study complements past studies in which lightning-flash rates were compared to the vertical structure of radar-inferred precipitation (Rutledge and Petersen 1994; Zipser and Lutz 1994; Petersen et al. 1996; Carey and Rutledge 1996; Petersen et al. 1999; Carey and Rutledge 2000).

Data and methodology

Advanced Lightning Direction Finder (ALDF) network

Four Advanced Lightning Direction Finder (ALDF) sensors were stationed across the MCTEX analysis region (Carey and Rutledge 2000). These sensors, developed by Global Atmospheric Inc. (GAI) and supplied by NASA/Marshall Space Flight Center (MSFC), detected the field strength, magnetic bearing, and time of arrival for lightning-induced radio emissions. This information allowed the location of ground strikes to be retrieved, along with other parameters. Similar to the devices described by Krider et al. (1976), these sensors consisted of a wideband system of two orthogonal magnetic loop antennas and a flat plate antenna. Based on the expected 80 to 90 per cent detection efficiency of the US National Lightning Detection Network (Cummins et al. 1998), we likewise assume 80 to 90 per cent detection efficiency for the ALDF network during the MCTEX.

Cloud-to-ground lightning locations and times of occurrence were supplied by the lightning research group at MSFC (R. Blakeslee, personal communication 1998). The accuracy of the derived stroke location depended on the stroke's proximity to the sensor

baselines, the type of retrieval algorithm used, and the number of independent time of arrival/magnetic bearing measurements utilised by the retrieval algorithm. Koshak et al. (2000) tested various algorithms on sets of computer-generated lightning sources over the Tiwi Islands and found positioning errors ranging from 1 to 10 km. The individual lightning strokes were grouped into flashes, assuming that strokes occurring within a short time interval (1 s) and distance (20 km) of each other belonged to the same flash.

Flat plate antenna

A Colorado State University flat plate antenna was installed at C-pol to detect the electrostatic field changes associated with both cloud-to-ground and in-cloud lightning, allowing us to estimate the total lightning-flash rate for storms near the antenna. The antenna consisted of a metallic plate which was oriented parallel to the ground (Uman 1987). Experience with the flat plate antenna in a variety of convective situations suggests that the maximum range for detecting most flashes is about 40 km (e.g. Carey and Rutledge 1996, 1998, 2000).

C-pol radar

The Bureau of Meteorology Research Centre/National Center for Atmospheric Research (BMRC/NCAR) C-band (5.3-cm) polarimetric/Doppler radar system (C-pol) was used during MCTEX (Keenan et al. 1998). This radar was capable of transmitting radiation of horizontal and vertical polarisation on a pulse-to-pulse basis. The pulse repetition frequency (PRF) was 1000 Hz, with 128 samples (64 horizontal, 64 vertical) collected for each gate. In addition to collecting the standard fields of horizontal reflectivity (Z_h), radial velocity (V_r), and spectral width (σ_v), C-pol also measured differential reflectivity (Z_{dr}), two-way total differential propagation phase shift (Ψ), and the coefficient of correlation at zero lag between the horizontally and vertically polarised backscattered echo ($|\rho_{hv}(0)|$). These polarimetric variables were obtained using the algorithms of Zahrai and Zrnicek (1993). A +0.1 dB bias in Z_{dr} was removed, as determined from a vertically pointing scan in stratiform precipitation on 29 November 1995 (Keenan et al. 1998). Propagation differential phase shift (φ_{dp}) was extracted from Ψ by taking a 13-gate running mean of Ψ along each ray of data. This smoothed Ψ field was accepted as φ_{dp} , and the difference between Ψ and φ_{dp} was attributed to backscatter differential phase shift, δ . The specific differential phase shift (K_{dp}) was obtained by taking the range derivative of φ_{dp} , and was calculated via a finite differencing method on a gate-to-gate basis. For a more thorough discussion of polarimetric vari-

ables available from C-pol see Keenan et al. (1998).

C-band attenuation issues

C-band radars are susceptible to significant attenuation in heavy rain (e.g. Sarchilli et al. 1993; Carey et al. 2000). This attenuation must be quantified before using the radar data for rain-rate estimates or hydrometeor identification. A first-order attenuation correction was applied to Z_h and Z_{dr} data using φ_{dp} . φ_{dp} is immune to attenuation and is independent of radar calibration errors (e.g. Zrnice and Ryzhkov 1996). We will outline the procedure below.

At weather radar wavelengths, specific attenuation (A_h (dBZ km⁻¹)) is approximately linearly proportional to K_{dp} (deg km⁻¹) (Bringi et al. 1990):

$$A_h \approx a \cdot K_{dp} \quad \dots 1$$

We assume a is constant and integrate Eqn 1 over the two-way propagation path. This yields

$$2 \int_r^{r'} A_h dr' \approx 2a \int_r^{r'} K_{dp} dr' \quad \dots 2a$$

$$-2 \int_r^{r'} \frac{\partial(Z_h)}{\partial r} dr' \approx -2a \int_r^{r'} \frac{\partial(\varphi_{dp})}{\partial r} dr' \quad \dots 2b$$

$$-\left[Z_h(r_2) - Z_h(r_1) \right] \approx a \left[\varphi_{dp}(r_2) - \varphi_{dp}(r_1) \right] \quad \dots 2c$$

The constant of proportionality, a , was derived experimentally for each radar volume by finding the negative of the slope of the best-fit line for a scatterplot of observed Z_h - φ_{dp} values (Ryzhkov and Zrnice 1995; Carey et al. 2000).

As in Carey et al. (2000), the linear regression analysis was limited to radar volumes within the height region 0.5-2 km above ground level (AGL), with $1 < K_{dp} < 2$ deg km⁻¹, $|\rho_{hv}(0)| > 0.95$, and $|\delta| < 5^\circ$. These restrictions eliminated outliers from the Z_h - φ_{dp} scatterplot, preventing radar volumes characterised by frozen precipitation, Mie scattering, or noisy data from biasing the estimate of the constant of proportionality, a .

The constant of proportionality between Z_{dr} and φ_{dp} (b) was obtained in similar fashion so that Z_{dr} could be corrected for differential attenuation. Corrected Z_h and Z_{dr} fields were then constructed using the relations:

$$Z_h^{(actual)} \approx Z_h^{(observed)} + a \cdot \varphi_{dp} \quad \dots 3$$

$$Z_{dr}^{(actual)} \approx Z_{dr}^{(observed)} + b \cdot \varphi_{dp}$$

Carey et al. (2000) extended the empirical method of Ryzhkov and Zrnice (1995) by including a 'large drop correction'. This accommodated the upward spikes in a and b found in very large drop cores (e.g.

$Z_{dr} \geq 3$ dB). This second-order correction was not applied to the radar data used in this study, but this is not expected to affect our main results.

C-pol hydrometeor identification

In regions where observed reflectivity ($Z_{h,total}$) exceeded 35 dBZ, $Z_{h,total}$ was partitioned into rain and graupel contributions. This was accomplished using difference reflectivity, Z_{dp} (Golestani et al. 1989). The theory is summarised below. For reference,

$$Z_{dp} [dB] = 10 \log (Z_h - Z_v) \quad \dots 4$$

where Z_h and Z_v are the reflectivity factors [mm⁶ m⁻³] at horizontal and vertical polarisation, respectively. Spherical targets do not affect Z_{dp} because they have equal horizontal and vertical reflectivity factors. For several reasons, frozen hydrometeors can be treated as spheres. First of all, hail and graupel particles tend to tumble as they fall (Pruppacher and Klett 1997). Secondly, for small oblate or prolate targets, polarised reflectivity is only sensitive to particle shape if the dielectric constant is large (Battan 1973). Since ice particles have a low dielectric constant, deviations from sphericity are less discernible to the polarimetric radar. As mentioned by Battan (1973), the ice particles can be effectively treated as equivolume spheres. This diminishes the impact that ice particles have on Z_{dp} . Since Golestani et al. found a nearly linear relationship between Z_{dp} and Z_h for simulated gamma raindrop-size distributions, Z_{dp} can be used to estimate horizontal reflectivity due solely to rain ($Z_{h,rain}$). As reasoned above, estimation of $Z_{h,rain}$ may be done in mixed-phase conditions in which rain and ice particles coexist. The particular relationship derived for this study was

$$Z_{h,rain} [dBZ] = 0.77 Z_{dp} + 14.0 \quad \dots 5$$

The method used to obtain this relationship is described in Carey et al. (2000).

Where $Z_{h,total} > 35$ dBZ, we subtracted $Z_{h,rain}$ from the total reflectivity (both in mm⁶m⁻³) and hence isolated the reflectivity due to graupel:

$$Z_{h,grpl} = Z_{h,total} - Z_{h,rain} \quad \dots 6$$

Then $Z_{h,grpl}$ was used to estimate M_{grpl} , the graupel mixing ratio (g kg⁻¹) via

$$M_{grpl} = 1000\pi \frac{\rho_{ice}}{\rho_{air}} N_0^{3/7} \left(5.28 \times 10^{-18} \frac{Z_{h,grpl}}{720} \right)^{4/7} \quad \dots 7$$

This M_{grpl} vs $Z_{h,grpl}$ equation was derived by assuming Rayleigh-Gans scattering. In the scattering simulations an inverse exponential particle-size distribution was assumed. N_0 was the intercept parameter of the size distribution (4×10^6) and ρ_{ice} was the densi-

ty of solid ice (917 kg m^{-3}).

In regions where $Z_{h,total} < 35 \text{ dBZ}$ the hydrometeors were assumed to be rain below the 0°C level and small ice crystals above the 0°C level.

Rain water content (g kg^{-1}) was quantified using $Z_{h,rain}$ (mm^6m^{-3}):

$$Z_{rain} = 3.01 \times 10^{-4} (Z_{h,rain})^{0.846} \quad \dots 8$$

This equation was based on T-matrix scattering simulations (Barber and Yeh 1975) using raindrop populations with drop-size distributions (DSDs) based on MCTEX disdrometer observations.

Description of MCTEX region

Island characteristics

The Tiwi Islands are located approximately 50 km north of Darwin in the extreme southeastern tip of the ‘maritime continent’ (Ramage 1968). The Tiwi’s are comprised of two islands separated by a narrow tidal channel (Fig. 1). Bathurst I. is the smaller of the two and is situated to the west of Melville I. Together, these islands stretch about 150 km from east to west and 65 km from north to south. Close to the southern coast of Melville I., a narrow ridge 50–100 m above sea level roughly parallels the coast. To the north, the topography gradually descends to the sea (Keenan et al. 1996a).

Climate

During the austral winter the intertropical convergence zone (ITCZ) is north of the islands and dry southeasterly winds from the Australian continent suppress precipitation. Typically, by November or December, the equatorial trough migrates far enough south to influence northern Australia, and the moist unsettled weather associated with the monsoon trough eventually pervades the region. Hence, the islands experience pronounced wet and dry seasons. Monsoonal bursts of deep westerly flow occur during this period in association with the Madden-Julian oscillation (Madden and Julian 1994). These westerly periods are commonly interrupted by ‘breaks’ during which the low to mid-level flow shifts to drier easterlies. During these interludes, widespread stratiform precipitation with embedded convection gives way to afternoon convective cloud complexes, including island thunderstorms (Keenan and Carbone 1992). These ‘break’ periods are similar to the ‘transition’ period that occurs at the end of the dry season before the austral summer monsoon establishes itself across northern Australia. It is during this ‘transition’ period that the MCTEX was conducted. Climatologically, island thunderstorms develop on 65–90 per cent of the days from

November–December (Keenan et al. 1990).

Convective organisation of case study days

Choice of case study days

In ranking potential case study days for this study, high marks were given to days uncomplicated by monsoonal influences. Fortunately, MCTEX provided many such days. Another important consideration was the quality and availability of radar and lightning data. In order to extract meaningful relationships between storm hydrometeor content and lightning-flash rate, timely volumetric scans should be available for all cells within detection range of the lightning sensors. This was not always possible when storms moved directly above the radar. This situation also compromised total lightning-flash rate measurements, as raindrops hitting the flat plate antenna caused spuriously high apparent flash rates. November 23 and 27 were chosen because they were excellent examples of diurnally forced island convection. The radar coverage and lightning data were also quite good.

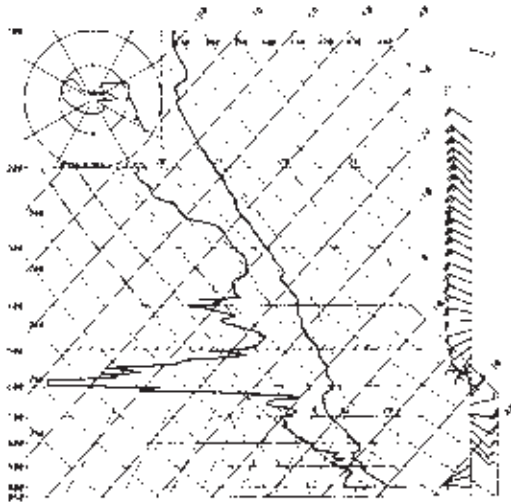
23 November 1995 case study

On 23 November 1995, light southerly low-level flow existed over the Tiwi Islands, attributable to an anticyclone to the west. This southerly flow converged with southeasterly winds east of Darwin and merged with westerly equatorial flow west of New Guinea. At the 700 hPa level (often considered the steering level for storms in this region), the wind was south-southeast at about 10 m s^{-1} . A broad region of 500 hPa anticyclonic flow just to the west of New Guinea was situated to the north of a 500 hPa band of westerlies ($5\text{--}10 \text{ m s}^{-1}$) centered about 2° south of the Tiwi Islands. A major upper-level trough over western Australia was pushing east, forging brisk northwesterly flow over the Tiwi islands above 400 hPa. These winds were supplemented by the strong subtropical jet ahead of the trough which had an entrance region about 8° south of the islands (Keenan et al. 1996b).

The thermodynamic profile shown in Fig. 2 was measured by a rawinsonde launched at 1036 local standard time LST (0106 UTC) from Melville Island (see Fig. 1). Light westerly winds were present in the lowest 1 km, with $5\text{--}7 \text{ m s}^{-1}$ southeasterly flow near 3 km AGL. Above the subsidence inversion at 600 hPa, the wind direction shifted to northwest and increased to 15 m s^{-1} in association with the entrance region of the subtropical jet over northern Australia.

By early afternoon, convective available potential energy (CAPE; 500 m mixed layer) had reached $1508 \text{ m}^2 \text{ s}^{-2}$ and the lifted index (LI) was -2°C . These indices were close to average values for the Darwin

Fig. 2 Skew T-ln p diagram with dew-point and temperature ($^{\circ}\text{C}$) on the abscissa and pressure (hPa) on the ordinate. Rawinsonde launched from Maxwell Creek, Melville I. at 0106 UTC on 23 November 1995. Horizontal wind barbs (knots) displayed on right side of figure. Full and half flags represent 10 kn and 5 kn, respectively.



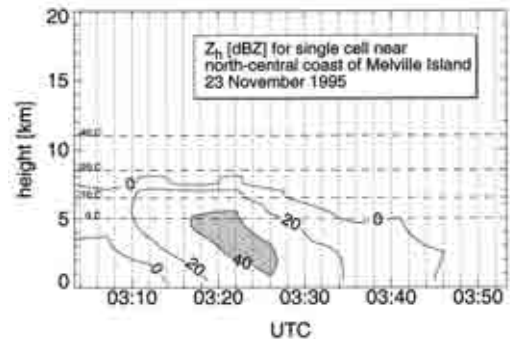
region (Keenan et al. 1990).

The combination of moderate instability and weak low-level wind shear did not favour long-lived deep convection on 23 November. The bulk Richardson number R (calculated as in Keenan et al. 1990) of 494 favoured unsteady, multicellular convective systems (Weisman and Klemp 1982, 1984, 1986).

Early development over northeast Melville I. Cells over northeast Melville I. quickly overcame the local convective inhibition and merged into an early afternoon thunderstorm complex. These early cells were in a most favoured position over the Tiwi Islands due to the enhanced low-level convergence between the west-southwest surface wind and the east coast sea-breeze. Carbone et al. (2000) and Laird et al. (1995) also noted the importance of narrow peninsulas (< 20 km) and sea-breeze front convergence in initiating early precipitating convection.

Isolated cells over western half of islands. Unlike northeastern Melville, convection over the western half of the islands was rather benign early in the afternoon. A time-height cross-section of horizontal reflectivity through a representative cell is shown in Fig. 3. In these cells, the height of the 30 dBZ reflectivity

Fig. 3 Time-height section of horizontal reflectivity (Z_h) (dBZ) through an early afternoon cell that developed over a narrow peninsula of northwest Melville I. on 23 November 1995. Dashed horizontal lines show environmental temperature levels.



surface never exceeded the -10°C isotherm level for more than a few minutes. Petersen et al. (1996) have shown that oceanic cells only electrify to the point of producing lightning when their 30 dBZ reflectivity surfaces maintain heights colder than the -10°C isotherm for approximately 10-15 minutes.

Other shallow cells developed near Apsley Strait between the west and south coast sea-breezes. These cells only precipitated for about 30 minutes, but they appeared to generate cold pools that spread out radially at the surface as they propagated to the northeast with the synoptic flow of 2 m s^{-1} . The edges of the cool pools were marked by a barely discernible enhancement in the reflectivity field that propagated outward from the precipitation echoes. The radar could detect these subtle features due to elevated concentrations of insects and a sharp gradient of refractive index along the boundaries (Wilson and Schreiber 1986). Carbone et al. (1997; 2000) found that similar shallow cool pools within the heated interior island boundary layer were 0.5-1 per cent negatively buoyant with respect to the undisturbed island boundary layer. The Ranku Community automated weather station (RANK AWS; see Fig. 1 for location) detected a $1\text{-}2^{\circ}\text{C}$ temperature drop coincident with the passage of the clear-air reflectivity line (0541 UTC). The surface winds also shifted from west to southwest and briefly gusted to 5 m s^{-1} . The Maxwell Creek (MAXW) AWS was affected by the rain-cooled air (no rain was recorded at either site, however) from 0420-0430 UTC. At this station, the temperature dropped by 3°C and the wind profiler detected a surge in southwesterly winds at 4 km elevation when the

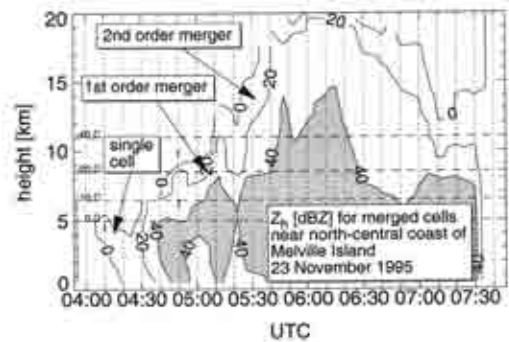
cells were directly above the site (0430 UTC). The speed of propagation for the radar echoes was consistent with the speed of a density current after taking into consideration detrainment, surface drag, viscosity and ambient wind (Simpson 1997). The precipitating cells probably modified the sub-cloud layer with evaporatively cooled downdraughts and appeared to trigger deep convection when they approached the north coast sea-breeze front. This was probably due to enhanced low-level convergence.

First-order merger. Between 0400 and 0500 UTC the north sea-breeze front was clearly distinguishable in the clear-air radar reflectivity data. MCTEX field observers also noted cloud street-like organisation of the radar echoes over the centre of the Tiwi Islands with some evidence for horizontal convective rolls aligned northwest to southeast. Longitudinal rolls within the boundary layer may have modified the sea-breeze circulation in a manner similar to that described by Atkins et al. (1995) in their study of a Florida sea-breeze. If so, this would create preferred regions for updraught development along the sea-breeze front prior to interaction with cold pool outflow boundaries.

A time-height section of horizontal reflectivity for cells near the north coast sea-breeze front is provided in Fig. 4. Similar to the cell in Fig. 3, most of the precipitation initially developed below the 0°C level through warm-rain processes. From 0405–0430 UTC, the bulk of the rain descended to the surface. By 0450 UTC, the shallow precipitating cells from the southwest drew closer, and as they approached, a rejuvenated updraught was initiated between them. Doppler velocity suggested brisk low-level inflow to cells along the sea-breeze front and to the cells a few kilometers to their south (0505 UTC). Soon the southern cells, having unrestricted access to island boundary-layer air, grew and engulfed cells along the sea-breeze. This merger was coincident with a surge in radar cloud-top height from 7 to 11 km altitude (0440–0455 UTC in Fig. 4). A combination of outflow collisions and differential motion of cloud masses enhanced the low-level convergence and supported rapid storm growth after 0500 UTC.

Second-order merger. By 0512 UTC, heavy rain ($Z_h > 45$ dBZ) reached the surface in the merged cells over north-central Melville I. Straddling the north coast sea-breeze front, these cells produced a downdraught that forced new convective development where it intersected the sea-breeze front. On the west side of the downdraught, the cells merged with additional convection along the north coast sea-breeze front and produced an intense convective complex

Fig. 4 Time-height section of Z_h (dBZ) for a cell along the north coast sea-breeze front (23 November 1995). Beyond 0515 UTC, the time-height section applies to a cluster of merged cells adjacent to the original cell. The drop in reflectivity near 0515 UTC is due to a shift in focus to an adjacent cell at a slightly earlier developmental stage. Dashed horizontal lines show environmental temperature levels.

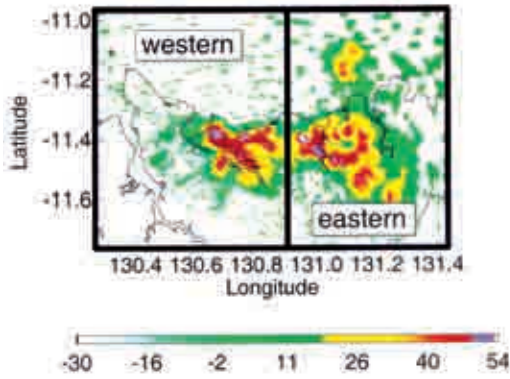


with echo tops to 18 km AGL. On the east side, the gust front collided with the outflow from the earlier storm over far northeast Melville I. The collision of these two cold pools along the sea-breeze front spawned an intense cell with a radar echo top of 20 km AGL (0540 UTC). The time-height section of reflectivity for this merged cell is depicted in the latter stage of the time series shown in Fig. 4.

Figure 5 shows a horizontal cross-section of reflectivity at 2 km AGL from the two major convective systems over northern Melville I. at 0541 UTC. Two regions were defined (western and eastern in Fig. 5) so that separate comparisons of lightning-flash rate and microphysical evolution could be made (next section).

The second-order merged cell in the eastern region was especially vigorous. Doppler velocity profiles near the core of the storm suggested strong convergence from the surface up to 6 km. This, in addition to the divergent radial flow in the upper levels provided evidence for a strong updraught. The mass continuity equation was used to make a rough estimate of vertical velocity. Radial divergence along the radar beam path was chosen to represent the horizontal divergence and a vertical profile of horizontal mass divergence was then constructed. Depending on the length of the radial segment over which the divergence was estimated and the boundary condition used ($w = 0$ at the ground or at the top of the storm), the maximum updraught speed was 35–40 m s^{-1} . Modelling studies of Tiwi I. thunderstorms have suggested similar values for maximum updraught speed (Golding 1993; Simpson et al. 1993; Keenan et al. 1994b; Crook 1997) and the value is reasonable con-

Fig. 5 Plan view of Z_h (dBZ) at 2 km AGL for 0541 UTC 23 November 1995. The western and eastern regions each encompass one distinct area of deep convection. Hydrometeor identification statistics and lightning-flash rates were compiled for each region.

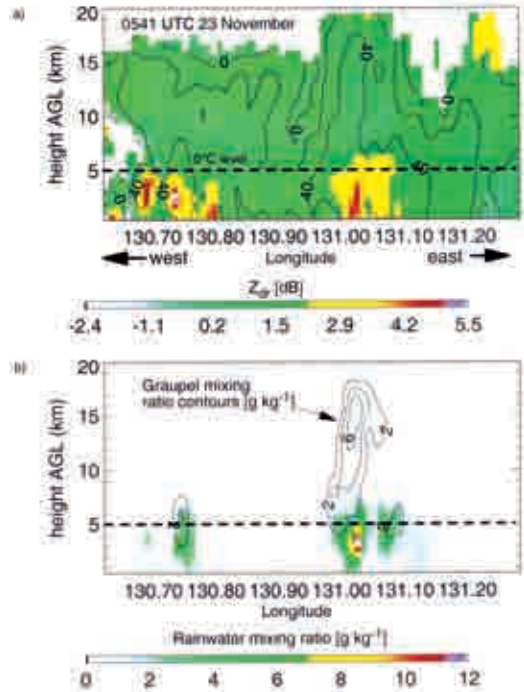


sidering the CAPE for this day ($\sim 1500 \text{ J kg}^{-1}$).

Figure 6(a) shows an E-W vertical cross-section of Z_h and Z_{dr} through this second-order merged cell. Horizontal reflectivity greater than 40 dBZ and near-zero values of Z_{dr} suggest high graupel concentrations above the freezing level (Fig. 6(b)). Just beneath these columns of graupel, but still above the freezing level, positive Z_{dr} values highlight probable regions of supercooled rainwater* (Fig. 6(b)).

Dissipative stage. After 0700 UTC, the main storms rapidly weakened and collapsed. Relatively weak precipitating cells continued to form along the north-western edge of the spreading island-scale cold pool. This side of the cold pool continued to intercept unperturbed island boundary-layer air, and the forced updraughts benefited from the environmental wind profile. Rotunno et al. (1988) showed that the optimal condition for a vertically erect and strong updraught along a gust front exists when the low-level vertical wind shear balances the horizontal vorticity generated by the buoyancy gradient across the cold pool. Along the southeastern edge of the cold pool, the environmental shear augmented the horizontal vorticity gen-

Fig. 6 East-west vertical cross-section (-11.4° latitude) through intense part of thunderstorm at 0541 UTC on 23 November. A plan view of Z_h for this time is shown in Fig. 5. Displayed in (a) are Z_h (dBZ) (contoured) and Z_{dr} (dB). Displayed in (b) are graupel mixing ratio (g kg^{-1}) (contoured) and rainwater mixing ratio (g kg^{-1}). Note the high graupel concentration above regions where rain is found above the 0°C level. See text for explanation of rainwater above the -40°C level.



* This figure also indicates a small amount of rainwater between 11 and 18 km AGL. This is physically unrealistic since pure water cannot exist in the liquid phase below -40°C ($\sim 11 \text{ km}$). Normal variance of Z_h and Z_{dr} about their actual values can account for this rainwater signature. For example, an overestimate of Z_{dr} by 0.2 dB would result in 0.5 g kg^{-1} of 'apparent rainwater' (based on 45 dBZ and zero Z_{dr}). This is a common type of error, but its overall effect on our results is probably negligible.

erated by the density current, so the surface air was probably swept behind the cold pool by a highly slanted updraught and entrained into its wake, never attaining its level of free convection. On the north-western side, the updraughts were sufficient to produce precipitation. These precipitating cells did not last very long since they were rapidly undercut by the advancing cold pool. The weak steering level flow on this day resulted in minimal vertical wind shear and probably precluded strong redevelopment along the gust front. A cell will usually dissipate if it cannot remain close to the edge of its gust front (Weisman and Klemp 1986; Wilson and Megenhardt 1997). This finding is elaborated upon by Carbone et al. (2000) in their treatment of MCTEX convection.

27 November 1995 case study

We now shift our focus to the second case, providing a similar overview of environmental conditions and the lifecycle of convection. The dominant circulation feature on 27 November was a strong upper-level anticyclone centered 2° north of the Tiwi islands. Strong 200 hPa divergence accompanied this feature and its closed circulation extended down to 500 hPa. At 700 hPa, almost the entire northern coast of Australia was covered by a wide band of 5–10 m s^{-1} easterlies, and the surface winds varied from calm to light easterlies to the east of the Tiwi Islands (Keenan et al. 1996b).

The 2158 UTC Maxwell Creek sounding (not shown) indicated northeasterly near-surface flow (5–10 kn) situated beneath stronger easterly flow at the trade-wind level (20 kn). Above that, the wind direction backed to the west and dropped to 5–15 kn between the 300 and 150 hPa levels. The lifted index (LI) and CAPE (500 m mixed layer) were -3°C and $903 \text{ m}^2 \text{ s}^{-2}$, respectively. The bulk Richardson number (R) was 108. Another sounding taken near the initial deep convection (0258 UTC) exhibited a warmer and slightly drier surface mixed layer, but very similar stability indices (e.g. LI was -2°C , CAPE $703 \text{ m}^2 \text{ s}^{-2}$, and R 112). These conditions favoured unsteady multicellular convection (Weisman and Klemp 1982; 1984). It is important to realise that pre-storm soundings are not necessarily representative of the actual conditions experienced by the mesoscale convective system, so one must exercise caution when anticipating storm behaviour with the aid of a sounding. The value of R was lower for 27 November compared to 23 November, possibly leading to greater storm organisation (weak squall line vs short-lived multicell). Apparently the vertical wind shear on 27 November was enough to keep cell updraughts close to their gust fronts.

Light northeasterly surface winds ($< 5 \text{ m s}^{-1}$) encouraged initial convective development over Bathurst I. on this day. Numerical simulations of this case have replicated this phase fairly well (Crook 1997; Saito et al. 1997). Scattered small cells embedded in the east-northeast flow developed across the northern part of the islands and propagated towards the south coast sea-breeze front (Fig. 7(a)).

A distinct reflectivity fine-line propagated ahead of the precipitating cells. Similar to that seen on 23 November, the observed propagation speed of the line ($3\text{--}6 \text{ m s}^{-1}$) was consistent with that of a density current (Simpson 1997). Once these small showers and their accompanying reflectivity fine line converged with the well-defined southern sea-breeze front, the cells abruptly penetrated the 0°C level, with radar cloud tops surpassing 12 km AGL by 0350 UTC (Fig. 7(a)).

The east-west aligned complex of cells eventually organised into a squall line that reoriented itself north-south and propagated to the west (Figs 7(b)–(e)). Forward progress of individual elements was briefly more rapid, but the average motion of the entire system was about 10 m s^{-1} . This reflected the environmental wind between 850 and 700 hPa, similar to the findings of Keenan and Carbone (1992). Northeasterly surface winds kept the eastern edge of the cold pool quasi-stationary and advected the convectively unstable boundary-layer air from eastern Melville I. towards the edge of the cool pool. This fostered intermittent strong storms 30 km north-northeast of the radar through 0800 UTC (Figs 7(c)–(f)).

Microphysical and electrical behaviour

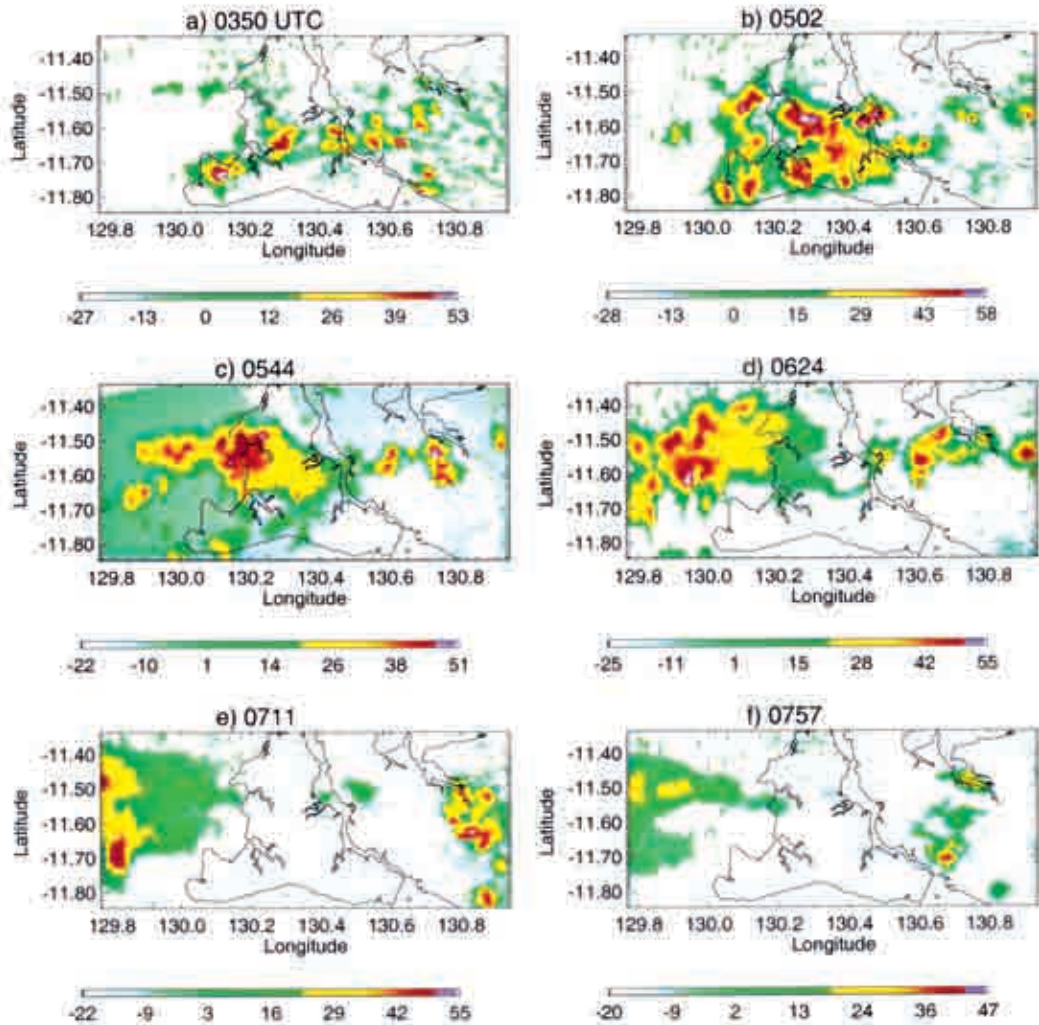
23 November 1995 case study

The electrical and microphysical history of the 23 November storms are summarised by the cloud-to-ground flash rate and mixed-phase graupel estimates shown in Fig. 8. On this day, the storms which formed over the Tiwi Islands were very electrically active. Cloud-to-ground flash rates peaked near 10 min^{-1} , and the total flash rate detected by the flat plate antenna exceeded 50 min^{-1} from 0550 to 0605 UTC.

Ideally, we would like to analyse individual storms and isolate the lightning-flash rate and microphysical characteristics for each group of cells. However, this is difficult to do in practice due to errors in lightning locations and ambiguities identifying specific cell boundaries using radar data. Hence the relationship between cloud-to-ground flash rate and mixed-phase graupel mass shown in Fig. 8 includes data from the total storm area. Cells at various stages of development are simultaneously contributing to the flash rate and graupel mass. Fortunately, it was possible to divide the convective activity on 23 November into two distinct areas (see Fig. 5). The cloud-to-ground flash rate and mixed-phase graupel associated with each region is displayed in Fig. 9. Unfortunately, polarimetric radar data were not available prior to 0523 UTC, so the build-up of mixed-phase graupel mass prior to the first cloud-to-ground lightning flash was not captured in the western storm (Fig. 9(a)). However, the evolution of the eastern convective region was sampled in its entirety (Fig. 9(b)). Interestingly, the cloud-to-ground peak flash rate peaks about 20 minutes after the mixed-phase graupel mass for this vigorous storm.

Although most of the cloud-to-ground lightning flashes were negative, there were several positive flashes for this case. Insight into the charge structure of these thunderstorms can be gained by inspecting

Fig. 7 Plan views of Z_h (dBZ) at 2 km AGL for 27 November (0350-0757 UTC).



the locations of the positive cloud-to-ground flashes relative to the negative cloud-to-ground flashes. On this day, the positive cloud-to-ground flashes typically occurred 10-20 km south-southeast of the negative cloud-to-ground flashes (Figs 10 and 11). Considering the strong upper-level winds from the northwest, it is likely that the positive ground flashes originated from a reservoir of positive charge in the upper levels of the storm. This would be consistent with the traditional dipole model of a thunderstorm. In the presence of wind shear, the positively charged ice crystals in the upper levels could have been displaced southeastward and exposed to ground. This would facilitate electrical breakdown between the

anvil and the Earth's surface. This 'tilted dipole' theory has been forwarded by several investigators as an explanation for positive cloud-to-ground flashes (e.g. Brook et al. 1982; Engholm et al. 1990; MacGorman and Nielsen 1991; Carey and Rutledge 1998).

27 November 1995 case study

The storms that developed during the second case study day (27 November) also formed in an environment of low wind shear. However, the atmosphere was more stable and the storms were characterised by less rainfall and lightning than on 23 November. Deep convection was initiated near the south and west coast sea-breeze fronts.

Fig. 8 Time series of mixed-phase graupel mass (solid) with 7-minute running average of cloud-to-ground flash rate (dashed line, right axis) for 23 November case. The vertical boundaries of the mixed-phase region are 5 km AGL (0°C) and 11 km (-40°C).

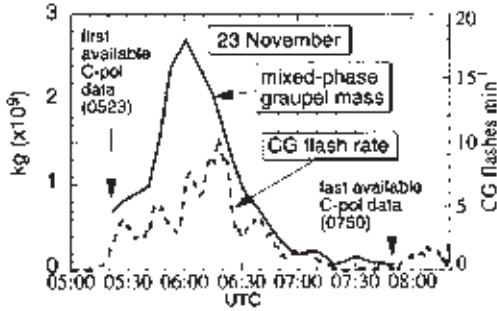
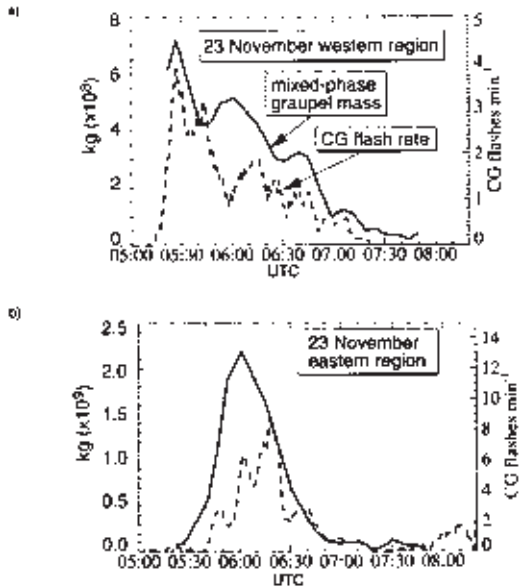


Fig. 9 As in Fig. 8, except for selected regions of the islands. Figure 5 shows the horizontal boundaries of the selected regions.



The cloud-to-ground flash rate detected near these storms is shown in Fig. 12. Peak cloud-to-ground flash rates were much less than on 23 November, reaching only 3 min^{-1} . Similarly to 23 November, the lightning rate appears to be strongly correlated to the graupel mass in the mixed-phase region. The five prominent peaks in mixed-phase graupel mass coin-

Fig. 10 Plan view of Z_h (dBZ) at 2 km AGL on 23 November at 0522 UTC. Locations of negative (blue minuses) and positive (red pluses) cloud-to-ground flashes are shown. Asterisk denotes radar location and range rings are spaced every 20 km.

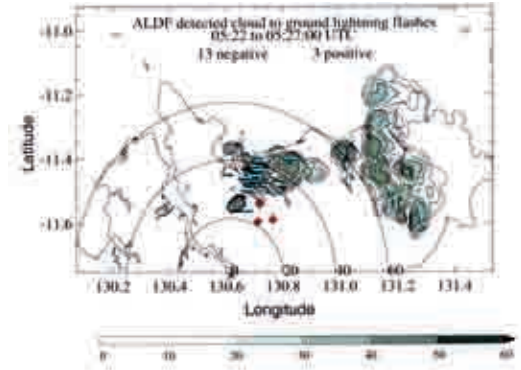


Fig. 11 As in Fig. 10 except for 0601 UTC.

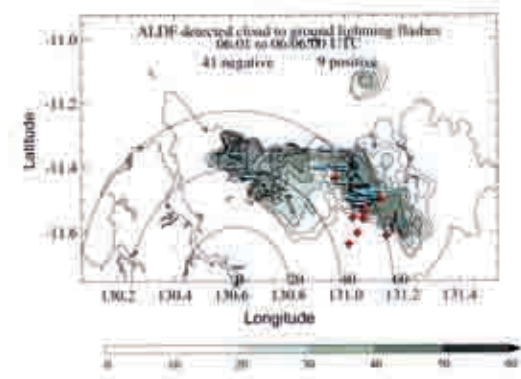
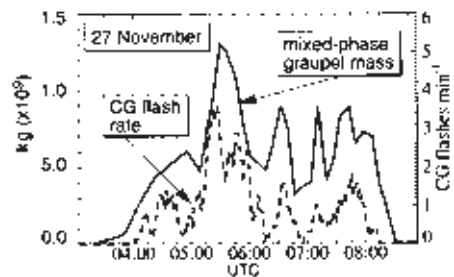


Fig. 12 As in Fig. 8 except for 27 November case.



cide extremely well with maxima in cloud-to-ground flash rate. For comparison, the cloud-to-ground flash rate is shown next to the rain mass flux* in Fig. 13. Notice how well the cloud-to-ground flash rate mimics the 20 to 40-minute fluctuations of graupel mass in the mixed-phase region (Fig. 12). On the other hand, the cloud-to-ground flash rate only loosely reflects the rain mass flux (Fig. 13).

Only five positive cloud-to-ground flashes were detected from the 27 November storms, and each flash was situated near a strong convective core. No positive cloud-to-ground flashes were associated with the stratiform precipitation trailing the weak squall line. However, the electric field mill sensor underneath this stratiform rain did indicate net positive charge aloft during this time. Observational studies have shown that this region is a preferred site for positive cloud-to-ground discharges (Rutledge and MacGorman 1988; Rutledge et al. 1993; Stolzenburg et al. 1994; Rutledge and Petersen 1994). Surprisingly, during MCTEX there were relatively few examples of positive cloud-to-ground flashes within the trailing stratiform precipitation of squall lines. The squall lines may have been too short-lived and weak to create much positive charge in the anvil through *in situ* mechanisms involving a well-established mesoscale updraught (Rutledge and MacGorman 1988; Rutledge et al. 1993; Stolzenburg et al. 1994; Rutledge and Petersen 1994). By the time most mesoscale convective systems matured, they already were on the verge of propagating off the Tiwi Islands. After they left the influence of the islands they often decayed rapidly over the cooler ocean waters.

Discussion

In November-December and during monsoon break periods, deep convection regularly occurs over the Tiwi Islands. In the early afternoon, shallow precipitating cells develop over the island interior and near the leeward coast sea-breeze front (Fig. 15). These cells produce weak cool pools that trigger deep convection along the sea-breeze front (Fig. 16). Rapid upscale development ensues after strong gust fronts from the deep convection collide near the sea-breeze front (Fig. 17). This results in a vigorous mesoscale convective system that quickly produces an extensive cold pool. New convective development is favoured along the downshear side of the cold pool (Fig. 18). The mesoscale system, in the form of a squall line, often propagates to the west with the surface to 700 hPa steering flow.

Fig. 13 Time series of storm total rain mass flux (kg s^{-1}) through 1 km AGL on 27 November. Cloud-to-ground flash rate is also shown (dashed; right axis).

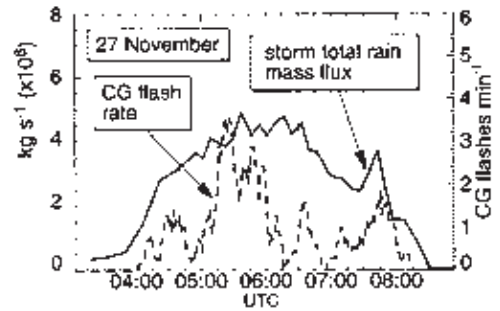
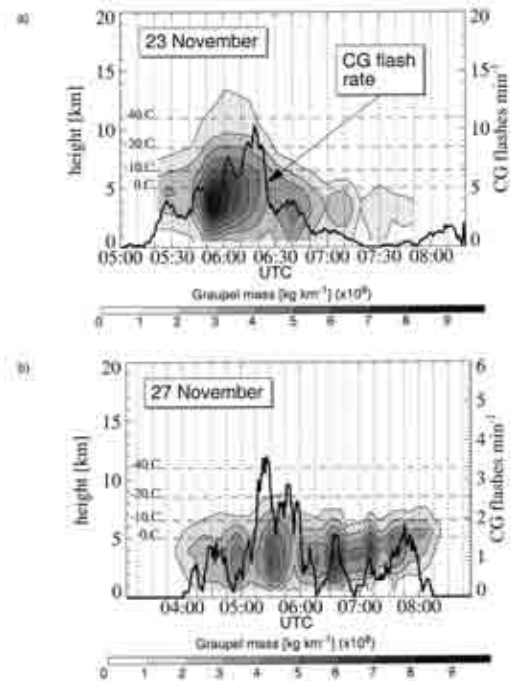


Fig. 14 Time-height contour plot of storm total graupel concentration (kg km^{-1}) for 23 November and 27 November. Seven-minute running average of cloud-to-ground flash rate (right axis) also shown. Graupel is found at much greater heights on 23 November than on 27 November. Note that the graupel algorithm becomes more sensitive to Z_h and Z_{dr} errors when Z_h is high. Typical radar uncertainty can account for graupel signature that appears well below the freezing level.



* Rain mass flux was estimated via the method described in Appendix D of Carey and Rutledge (2000).

Fig. 15 Over the Tiwi Islands, surface wind direction determines the dominant sea-breeze front. For example, if the wind is southerly, then the north coast sea-breeze front will be strongest. In the morning, shallow precipitating cells develop over the island interior and near the sea-breeze front. Pockets of evaporatively cooled air spread out beneath these cells.

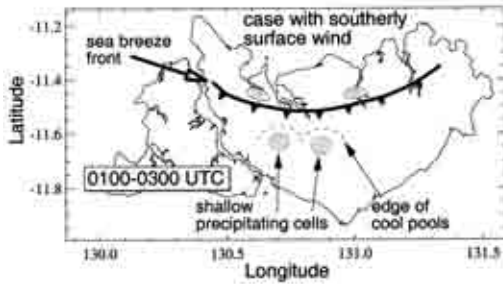


Fig. 16 As the pockets of cool air approach the sea-breeze front, first-order merged cells are triggered along the front.

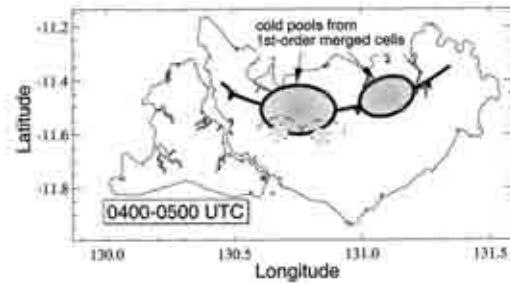


Fig. 17 Explosive vertical development ensues as strong gust fronts from the first-order cells collide near the sea-breeze front. This leads to a second-order merged cell.

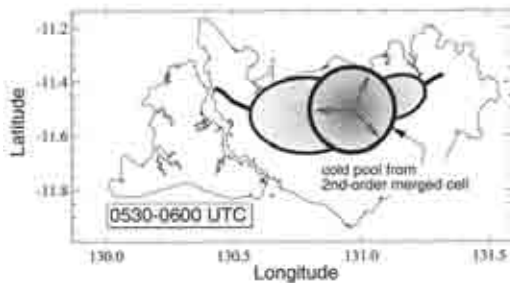
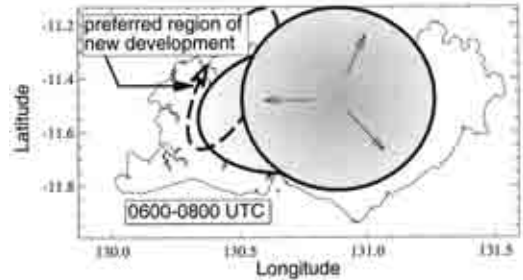


Fig. 18 A large cold pool envelops the islands as the second-order merged cell collapses. The low-level wind profile fosters further convective development on the downshear side of the cold pool. Typically, the western side is favored due to the easterly trade wind maximum near 700 hPa.



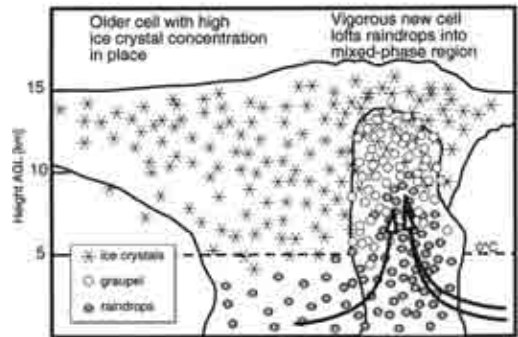
The radar and electrical findings for the two MCTEX case study days are consistent with NIC theory, specifically the strong association between precipitation-sized ice and lightning-flash rates. The flat plate antenna located at the radar site did not detect any cloud-to-ground or in-cloud lightning flashes until cells exhibited significant graupel signatures above the -10°C level. Warm rain precipitation processes were incapable of generating electrical field strengths necessary for lightning. The results of this study also suggest that graupel is an active participant in thunderstorm electrification and that the lightning-flash rate is a strong function of the amount of graupel above the freezing level. Graupel originates from supercooled raindrops lofted above the freezing level by strong updraughts (e.g. Bringi et al. 1997). The presence of supercooled drops above the 0°C level is clearly indicated by differential reflectivity (Z_{dr}) signatures. High graupel concentrations were usually found above areas that had significant rainwater above the 0°C level (see Fig. 6).

On 27 November, the cloud-to-ground lightning rate maxima occurred simultaneously with peaks in mixed-phase graupel mass. However, on 23 November the cloud-to-ground lightning peaked approximately 20 minutes after the mixed-phase graupel mass. This may be due to the delayed formation of a lower positive charge centre (Carey and Rutledge 1996). Previous studies have found that cloud-to-ground lightning is most prevalent when graupel which was previously suspended by an updraught descends below the 0°C level (Williams et al. 1989; Petersen et al. 1996; Carey and Rutledge 1996; 2000). According to laboratory studies (Takahashi 1978; Saunders et al. 1991), once the graupel descends below the ‘level of charge

reversal' the graupel should begin charging positively. This level resides between -10 and -22°C and is sensitive to the cloud water content, droplet size distribution and ice particle fallspeeds (Takahashi 1978; Jayaratne et al. 1983; Saunders et al. 1991; Williams et al. 1994). If the thunderstorm develops positively charged graupel beneath the main level of negative charge, this could promote the downward propagation of stepped leaders from the negative charge region. Instead of travelling upward toward the upper-level positive charge and creating an in-cloud discharge, the stepped leader could be drawn towards the surface, resulting in a cloud-to-ground flash (Clarence and Malan 1957). The delay between the cloud-to-ground flash rate peak and the graupel mass above the freezing level (20 minutes) observed on 23 November may be due to the strength of the updraught. Although there were no direct measurements of updraught strength, many aspects of the thunderstorm suggested a very strong updraught was present (e.g. Doppler velocity, CAPE, cloud-top height, vertical reflectivity structure). The strong updraught may have lofted the graupel high in the storm and delayed the formation of a lower positive charge centre. Comparison of the C-pol data from the two case study days shows that graupel was lofted to greater heights on 23 November than on 27 November (Fig. 14). As mentioned earlier, the downshear displacement of positive cloud-to-ground flashes on 23 November (Figs 10 and 11) suggested a normal polarity dipole was present (i.e. the primary region of positive charge was situated above the main negative charge layer). A lower positive charge layer could potentially develop from such a charge configuration. The 27 November thunderstorms probably did not have updraughts capable of elevating the graupel to extreme heights, possibly allowing their lower layers of positive charge to develop quickly and initiate cloud-to-ground lightning soon after graupel was created.

Over the Tiwi Islands, for our two MCTEX case study days, lightning was limited to merged cloud systems. Carey and Rutledge (2000) extend this finding to 28 November 1995. The merged convective cells were more vigorous than the isolated early morning shallow convection. With wider cloud bases, the merged cells experienced less entrainment, efficiently converting more surface-based instability to updraught strength. These updraughts were capable of lofting more raindrops and supercooled cloud water above the freezing level where the raindrops could become 'instant graupel'. New cells that formed near older convection may have merged with cloud regions already characterised by high ice particle concentrations (Fig. 19). The ice particles could then efficiently nucleate supercooled water within the new updraught, providing latent heat release and

Fig. 19 As a new cell develops and merges with an older cell, the supercooled raindrops lofted above the freezing level (dashed line) may be efficiently frozen by contact with ice crystals from the older cell. As graupel, these frozen raindrops could participate in NIC. The high ice crystal concentration would imply a high charging rate and would therefore promote lightning. This could explain the high lightning-flash rates observed with merged convective systems.



added buoyancy. The elevated ice crystal concentrations in the merged cell could also aid lightning production by allowing higher charging rates via NIC.

Acknowledgments

We would like to thank everyone who provided MCTEX datasets and various research suggestions, including Andrew Crook (NCAR), Tom Keenan (BMRC), Chris Burghart (NCAR), Jim Wilson (NCAR), Jeff Bailey (NASA/MSFC), Rit Carbone (NCAR) and Rich Blakeslee (NASA/MSFC). Ken Glasson (BoM) and Jon Lutz (NCAR) were instrumental in setting up and providing high quality data from C-pol. Thanks to all members of the CSU Atmospheric Science Radar Meteorology group for generous computer and research assistance. This material is based upon work supported under a National Science Foundation Graduate Fellowship awarded to David A. Ahijevych. Additional funding was provided by the NSF grant ATM-9726464 and the NASA TRMM grants NAG5-2692 and NAG5-4754.

References

- Atkins, N.T., Wakimoto, R.M. and Weckworth, T.M. 1995. Observations of the sea-breeze front during CaPE. Part II: Dual-Doppler and aircraft analysis. *Mon. Weath. Rev.*, 123, 944-69.
- Avila, E.E. and Caranti, G.M. 1994. A laboratory study of static

- charging by fracture in ice growing by riming. *J. geophys. Res.*, **99**, 10611–20.
- Barber, P. and Yeh, C. 1975. Scattering of electromagnetic waves by arbitrarily shaped dielectric bodies. *Appl. Opt.*, **14**, 2864–72.
- Battan, L.J. 1973. *Radar Observation of the Atmosphere*. Techbooks, 324 pp.
- Bringi, V.N., Knupp, K., Detwiler, A., Liu, L., Caylor, I.J. and Black, R.A. 1997. Evolution of a Florida thunderstorm during the Convection and Precipitation/Electrification Experiment: the case of 9 August 1991. *Mon. Weath. Rev.*, **125**, 2131–60.
- Bringi, V.N., Chandrasekar, V., Balakrishnan, N. and Zrnica, D.S. 1990. An examination of propagation effects in rainfall on radar measurements at microwave frequencies. *J. Atmos. Oceanic Tech.*, **7**, 829–40.
- Brook, M., Nakano, M., Krehbiel, P. and Takeuti, T. 1982. Electrical structure of the Hokuriku winter thunderstorms. *J. geophys. Res.*, **87**, 1207–15.
- Scripps Institute of Oceanography 1993. *CEPEX Experiment Design*. Center for Clouds, Chemistry and Climate, Scripps Institute of Oceanography, Univ. of California, San Diego.
- Carbone R.E., Wilson, J.W., Keenan, T.D. and Hacker, J.M. 2000. Tropical island convection in the absence of significant topography. Part I: Lifecycle of diurnally forced convection. *Mon. Weath. Rev.*, **128**, 3459–80.
- Carbone R.E., Keenan, T.D., Wilson, J.W. and Hacker, J.M. 1997. Boundary layer structures and the role of breezes in forcing deep island convection. *Preprints, 28th Conf. on Radar Meteor.*, Sept. 7–12, Austin, TX, Amer. Met. Soc., 565–6.
- Carey, L.D., Rutledge, S.A. and Ahijevych, D.A. 2000. Correcting propagation effects in C-band polarimetric radar observations of tropical convection using differential propagation phase. *Jnl appl. Met.*, **39**, 1405–33.
- Carey, L.D. and Rutledge, S.A. 1996. A multiparameter radar case study of the microphysical and kinematic evolution of a lightning producing storm. *Met. Atmos. Phys.*, **59**, 33–64.
- Carey, L.D. and Rutledge, S.A. 1998. Electrical and multiparameter radar observations of a severe hailstorm. *J. geophys. Res.*, **103**, 13979–4000.
- Carey, L.D. and Rutledge, S.A. 2000. The relationship between precipitation and lightning in tropical island convection: A C-band polarimetric radar study. *Mon. Weath. Rev.*, **128**, 2687–2710.
- Clarence, N.D. and Malan, D.J. 1957. Preliminary discharge processes in lightning flashes to ground. *Q. Jl R. Met. Soc.*, **83**, 161–72.
- Crook, N. A. 1997. Simulation of convective storms over the Tiwi Islands and comparison with observations from MCTEX. *Preprints, 22nd Conf. on Hurricanes and Tropical Meteor.*, May 19–23, 1997, Fort Collins, CO, 376–7.
- Cummins, K.L., Murphy, M.J., Jardo, E.A., Hiscox, W.L., Pyle, R.B. and Pifer, A.E. 1998. A combined TOA/MDF technology upgrade of the U. S. National Lightning Detection Network. *J. geophys. Res.*, **103**, 9035–44.
- Engholm, C.D., Williams, E.R. and Dole, R.M. 1990. Meteorological and electrical conditions associated with positive cloud-to-ground lightning. *Mon. Weath. Rev.*, **118**, 470–87.
- Gamache, J.F., Marks, F.D. Jr. and Burpee, R.W. 1987. *EMEX data report: The equatorial mesoscale experiment*. NOAA/Atlantic Oceanographic and Meteorological Laboratory, 4301 Rickenbacker Causeway, Miami, Florida, 33149.
- Golding, B.W. 1993. A numerical investigation of tropical island thunderstorms. *Mon. Weath. Rev.*, **121**, 1417–33.
- Golestani, Y., Chandrasekar, V. and Bringi, V.N. 1989. Intercomparison of multiparameter radar measurements. *Proc., 24th Conf. Radar Meteor.*, Tallahassee, FL, Amer. Meteor. Soc., 309–314.
- Holland, G.J., McBride, J.L., Smith, R.K., Jasper, D.J. and Keenan, T.D. 1986. The BMRC Australian Monsoon Experiment. *AMEX. Bull. Am. Met. Soc.*, **67**, 1466–72.
- Houze, R.A., Jr, Geotis, S.G., Marks, F.D. and West, A.K. 1981. Winter monsoon convection in the vicinity of North Borneo. Part I: Structure and time variation of the clouds and precipitation. *Bull. Am. Met. Soc.*, **109**, 1595–614.
- Janowiak, J.E., Krueger, A.F. and Arkin, P.F. 1985. Atlas of outgoing longwave radiation derived from NOAA satellite data. *NOAA Atlas No. 6*. U. S. Dept. of Commerce, Washington, D.C.
- Jayaratne, E.R., Saunders, C.P.R. and Hallett, J. 1983. Laboratory studies of the charging of soft-hail during ice crystal interactions. *Q. Jl R. Met. Soc.*, **109**, 609.
- Keenan, T.D., Ferrier, B. and Simpson, J. 1994b. Development and structure of a maritime continent thunderstorm. *Met. Atmos. Phys.*, **53**, 185–222.
- Keenan, T.D., Morton, B.R., Manton, M.J. and Holland, G.J. 1989. The Island Thunderstorm Experiment (ITEX): a study of tropical thunderstorms in the maritime continent. *Bull. Am. Met. Soc.*, **70**, 152–9.
- Keenan, T.D., Morton, B.R., Zhang, X.S. and Nyguen, K. 1990. Some characteristics of thunderstorms over Bathurst and Melville islands near Darwin, Australia. *Q. Jl R. Met. Soc.*, **116**, 1153–72.
- Keenan, T.D., Holland, G.J., Rutledge, S.A., Simpson, J., McBride, J., Wilson, J., Moncrieff, M., Carbone, R., Frank, W., Sanderson, B., Tapper, N. and Hallett, J. 1994a. Science plan Maritime Continent Thunderstorm Experiment (MCTEX), *BMRC Research Report 44*, Bur. Met., Australia, 61 pp.
- Keenan, T.D., Glasson, K., Cummings, F., Bird, T.S., Keeler, J. and Lutz, J. 1998. The BMRC/NCAR C-band polarimetric (C-POL) Radar System. *J. Atmos. Oceanic Tech.*, **15**, 871–86.
- Keenan, T.D., Puri, K., Mills, G. and Bowen, R. 1996b. Regional BMRC analyses of atmospheric circulation during MCTEX. *BMRC Research Report 57*, Bur. Met., Australia, 67 pp.
- Keenan, T.D., Carbone, R.E., Rutledge, S.A., Wilson, J., Holland, G.J. and May, P. 1996a. The Maritime Continent Thunderstorm Experiment (MCTEX): Overview and initial results. *Preprints, 7th Conf. on Mesoscale Processes*, Sept. 9–13, Reading, UK, Amer. Met. Soc., 326–328.
- Keenan, T.D. and Brody, L.R. 1988. Synoptic-scale modulation of convection during the Australian summer monsoon. *Mon. Weath. Rev.*, **116**, 71–85.
- Keenan, T.D. and Carbone, R.E. 1992. A preliminary morphology of precipitation systems in tropical northern Australia. *Q. Jl R. Met. Soc.*, **118**, 283–326.
- Keenan, T.D., Rutledge, S., Carbone, R., Wilson, J., Takahashi, T., May, P., Tapper, N., Platt, M., Hacker, J., Sekelsky, S., Moncrieff, M., Saito, K., Holland, G., Crook, A. and Gage, K. 2000. The Maritime Continent Thunderstorm Experiment (MCTEX): Overview and Some Results. *Bull. Am. Met. Soc. (accepted)*.
- Koshak, W.J., Blakeslee, R.J. and Bailey, J.C. 2000. Data retrieval algorithms for validating the optical transient detector and the lightning imaging sensor. *J. Atmos. Oceanic Tech.*, **17**, 279–97.
- Krider, E.P., Noggle, R.C. and Uman, M.A. 1976. Wideband magnetic direction finder for lightning return strokes. *Jnl appl. Met.*, **15**, 301–6.
- Krishnamurti, T.N., Kanamitsu, M., Koss, W.J. and Lee, J.D. 1973. Tropical east-west circulations during the northern winter. *J. Atmos. Sci.*, **30**, 780–7.
- Laird, N.F., Kristovich, D.A.R., Rauber, R.M., Ochs, H.T. III, and Miller, L.J. 1995. The Cape Canaveral sea and river breezes: kinematic structure and convective initiation. *Mon. Weath. Rev.*, **123**, 2942–56.
- Lau, K.-M., Chang, C.P. and Chan, P.H. 1983. Short-term planetary-scale interactions over the tropics and mid-latitudes. Part II: Winter-MONEX period. *Mon. Weath. Rev.*, **111**, 1372–88.
- MacGorman, D.R. and Nielsen, K.E. 1991. Cloud-to-ground lightning in a tornadic storm on 8 May 1986. *Mon. Weath. Rev.*, **119**, 1557–74.
- Madden, R.A. and Julian, P.R. 1994. Observations of the 40–50-day tropical oscillation: A review. *Mon. Weath. Rev.*, **122**, 814–37.
- Miller, M.J. and Betts, A.K. 1977. Travelling convective storms over Venezuela. *Mon. Weath. Rev.*, **105**, 833–48.
- Petersen, W.A., Carey, L.D., Rutledge, S.A., Knievel, J.C., Doesken, N.J., Johnson, R.H., McKee, T.B., Vondar Haar, T. and Weaver, J.F. 1999. Mesoscale and radar observations of the Fort Collins flash flood of 28 July 1997. *Bull. Am. Met. Soc.*, **80**, 191–216.

- Petersen, W.A., Rutledge, S.A. and Orville, R.E. 1996. Cloud-to-ground observations from TOGA COARE: selected results and lightning location algorithms. *Mon. Weath. Rev.*, 124, 602-20.
- Pruppacher, H.R. and Klett, J.D. 1997. *Microphysics of Clouds and Precipitation*, 2nd rev. and enl. ed. Kluwer Academic Publishers, 954 pp.
- Ramage, C.S. 1968. Role of a tropical 'maritime continent' in the atmospheric circulation. *Mon. Weath. Rev.*, 96, 365-70.
- Rasmusson, E.M. and Arkin, P.A. 1985. Interannual climate variability associated with the El Niño/Southern Oscillation. *Proc. Coupled Ocean-Atmosphere models*. Amsterdam: Elsevier Science Publishers B.V., 697-725.
- Reynolds, S.E., Brook, M. and Gourley, M. F. 1957. Thunderstorm charge separation. *J. Met.*, 14, 426-36.
- Rotunno, R., Klemp, J.B. and Weisman, M.L. 1988. A theory for strong, long-lived squall lines. *J. Atmos. Sci.*, 45, 463-85.
- Rutledge, S.A., Williams, E.R. and Keenan, T.D. 1992. The Down Under Doppler and Electricity Experiment (DUNDEE): Overview and Preliminary results. *Bull. Am. Met. Soc.*, 73, 3-16.
- Rutledge, S.A., Williams, E.R. and Petersen, W.A. 1993. Lightning and electrical structure of mesoscale convective systems. *Atmos. Res.*, 29, 27-53.
- Rutledge, S.A. and MacGorman, D.R. 1988. Cloud-to-ground lightning activity in the 10-11 June 1985 mesoscale convective system observed during the Oklahoma-Kansas PRE-STORM project. *Mon. Weath. Rev.*, 116, 1393-408.
- Rutledge, S.A. and Petersen, W.A. 1994. Vertical radar reflectivity structure and cloud-to-ground lightning in the stratiform region of MCS's: Further evidence for in-situ charging in the stratiform region. *Mon. Weath. Rev.*, 122, 1760-76.
- Ryzhkov, A. and Zrnich, D.S. 1995. Precipitation and attenuation measurements at a 10-cm wavelength. *Jnl appl. Met.*, 34, 2121-34.
- Saito, K., Keenan, T.D., Holland, G.J. and Puri, K. 1997. Numerical simulation of tropical diurnal thunderstorms over the Tiwi Islands. *Preprints, 22nd Conf. on Hurricanes and Tropical Meteor.*, May 19-23, 1997, Fort Collins, CO, 378-379.
- Saunders, C.P.R., Keith, W.D. and Mitzeva, R.P. 1991. The effect of liquid water on thunderstorm charging. *J. geophys. Res.*, 96, 11007-17.
- Scarchilli, G., Gorgucci, E., Chandrasekar, V. and Seliga, T.A. 1993. Rainfall estimation using polarimetric techniques at C-band frequencies. *Jnl appl. Met.*, 32, 1150-60.
- Simpson, J., Keenan, T.D., Ferrier, B., Simpson, R.H. and Holland, G.J. 1993. Cumulus mergers in the maritime continent region. *Met. Atmos. Phys.*, 51, 73-99.
- Simpson, J.E. 1997. *Gravity Currents in the Environment and the Laboratory*. 2d ed. Cambridge University Press, 244 pp.
- Skinner, T. and Tapper, N. 1994. Preliminary sea breeze studies over Bathurst and Melville Islands, Northern Australia, as part of the Island Thunderstorm Experiment (ITEX). *Met. Atmos. Phys.*, 53, 77-94.
- Sommeria, G. and Testud, J. 1984. COPT81: A field experiment for the study of dynamics and electrical activity in continental tropical regions. *Bull. Am. Met. Soc.*, 65, 4-10.
- Stolzenburg, M., Marshall, T.C., Rust, W.D. and Smull, B. F. 1994. Horizontal distribution of electrical and meteorological conditions across the stratiform region of a mesoscale convective system. *Mon. Weath. Rev.*, 122, 1777-97.
- Takahashi, T. 1978. Riming electrification as a charge generation mechanism in thunderstorms. *J. Atmos. Sci.*, 35, 1536-48.
- Uman, M.A. 1987. *The Lightning Discharge*. Academic Press, New York, 377 pp.
- Webster, P.J. and Houze, R.A. 1991. The Equatorial Mesoscale Experiment (EMEX): An overview. *Bull. Am. Met. Soc.*, 72, 1481-505.
- Webster, P.J. and Lukas, R.R. 1992. The TOGA Coupled Ocean-Atmosphere Response Experiment. *Bull. Am. Met. Soc.*, 73, 1377-416.
- Weisman, M.L. and Klemp, J.B. 1982. The dependence of numerically simulated convective storms on vertical wind shear and buoyancy. *Mon. Weath. Rev.*, 110, 504-20.
- Weisman, M.L. and Klemp, J.B. 1984. The structure and classification of numerically simulated convective storms in directionally varying wind shears. *Mon. Weath. Rev.*, 112, 2479-98.
- Weisman, M.L. and Klemp, J.B. 1986. *Characteristics of Isolated Convective Storms. Mesoscale Meteorology and Forecasting*. Ed. P. S. Ray, Amer. Met. Soc., 331-358.
- Williams, E.R., Weber, M.E. and Orville, R.E. 1989. Relationship between lightning type and convective state of thunderclouds. *J. geophys. Res.*, 94, 13213-20.
- Williams, E.R., Zhang, R. and Boccippio, D. 1994. Microphysical growth state of ice particles and large-scale electrical structure of clouds. *J. geophys. Res.*, 99, 10787-92.
- Williams, E.R., Geotis, S.G., Renno, N., Rutledge, S. A., Rasmussen E. and Rickenbach, T. 1990. Hot towers in the tropics. *Preprints, AMS Conference on Atmospheric Electricity*, October 22-26, 1990, Kananaskis Provincial Park, Alberta, Canada.
- Wilson, J.W. and Megenhardt, D.L. 1997. Thunderstorm initiation, organization, and lifetime associated with Florida boundary convergence lines. *Mon. Weath. Rev.*, 125, 1507-25.
- Wilson, J.W. and Schreiber, W.E. 1986. Initiation of convective storms at radar-observed boundary-layer convergence lines. *Mon. Weath. Rev.*, 114, 2516-36.
- Zahrai, A. and Zrnich, D.S. 1993. The 10-cm wavelength polarimetric weather radar at NOAA's National Severe Storms Laboratory. *J. Atmos. Sci.*, 10, 649-62.
- Zipser, E.J. and Lutz, K.R. 1994. The vertical profile of radar reflectivity of convective cells: A strong indicator of storm intensity and lightning probability? *Mon. Weath. Rev.*, 122, 1751-9.
- Zrnich, D.S. and Ryzhkov, A. 1996. Advantages of rain measurements using specific differential phase. *J. Atmos. Oceanic Tech.*, 13, 454-64.

Subtropical fronts observed during the 1996 Central Australian Fronts Experiment

Michael J. Reeder

Department of Mathematics and Statistics, Monash University, Australia

Roger K. Smith

Meteorological Institute, University of Munich, Germany

Roger Deslandes

Bureau of Meteorology Training Centre, Australia

Nigel J. Tapper

School of Geography and Environmental Science, Monash University, Australia

and

Graham A. Mills

Bureau of Meteorology Research Centre, Australia

(Manuscript received January 2000; revised May 2000)

The 1996 Central Australian Fronts Experiment (CAFE96) was the third in a series of field experiments designed to better understand the structure and dynamics of late dry-season subtropical cold fronts that affect central Australia. In this paper, the behaviour of three fronts observed during CAFE96 are described in detail and the four other fronts that occurred are examined in the light of previous studies.

In total, fourteen fronts were documented during the three field experiments, of which twelve crossed central Australia during the evening or early hours of the morning. Only one of the fourteen crossed central Australia during the late afternoon (Event 4 in CAFE96), and only one in the mid-morning (Event 6 in CAFE96). The latter front arrived at Alice Springs during the mid-morning and, as the daytime turbulent mixing increased, it ceased advancing northeastward and retrogressed. It subsequently retreated through Alice Springs, giving way to strong northwesterly winds and blowing dust. The front reversed direction once again and was observed at a station 70 km southeast of Alice Springs during the mid-afternoon. While it is probably quite common for the position of subtropical cold fronts to oscillate back and forth as the daytime turbulent mixing waxes and wanes, Event 6 is the first example to be documented in detail. Event 3 is more typical of the fronts observed in the two previous experiments, but is discussed briefly here because it is the best example to date exhibiting near-surface warming in a strip following the passage of the cold front. This warming was detected in satellite imagery and confirmed by surface measurements.

Introduction

Cold fronts frequently migrate equatorwards across Australia, penetrating deep into the subtropics. They

regularly reach as far north as the Gulf of Carpentaria (around 17°S), and occasionally push northward of Darwin (12°S). (The locations of places named in the text are shown in Fig. 1.) The synoptic environment of these fronts is similar to that of the summertime cool change of southeastern Australia (Reeder and

Corresponding author address: M.J. Reeder, Department of Mathematics and Statistics, Monash University, Clayton, Vic. 3800, Australia.

Email: michael.reeder@sci.monash.edu.au